

Camera Calibration for Daylight Specular-Point Locus

Mark S. Drew¹, Hamid Reza Vaezi Joze¹, and Graham D. Finlayson²

¹*School of Computing Science, Simon Fraser University,
Vancouver, B.C., Canada V5A 1S6*

²*School of Computing Sciences, The University of East Anglia,
Norwich, U.K., NR4 7TJ*

April 2012

In this paper we present a new camera calibration method aimed at finding a straight-line locus, in a special colour feature space, that is traversed by daylights and as well also approximately followed by specular points. The aim of the calibration is to enable recovering the colour of the illuminant in a scene, using the calibrated camera. First we prove theoretically that any candidate specular points, for an image that is generated by a specific camera and taken under a daylight, must lie on a straight line in log-chromaticity space, for a chromaticity that is generated using a geometric-mean denominator. Use is made of the assumptions that daylight illuminants can be approximated using Planckians and that camera sensors are narrowband or can be made so by spectral sharpening. Then we show how a particular camera can be calibrated so as to discover this locus. As applications we use this curve for illuminant detection, and also for re-lighting of images to show they would appear under lighting having a different colour temperature.

1. Introduction

The objective of this paper is to show that natural lights must necessarily follow a straight-line locus, in a special 2-D chromaticity feature space generated using a geometric-mean denominator to remove the effect of magnitude from colour, and that this locus can be derived from a camera calibration. Transformed back into non-log coordinates, the straight line in log colour space means that in terms of ordinary L_1 -norm based chromaticity $\{R, G\}/(R + G + B)$ lights follow a particular curve. The locus determined is camera-dependent. Derivation of the parameters of this locus via a camera calibration means that then one can use the path to help identify the illuminant in the scene, and also to transform from one illuminant to another.

In this paper, the main use we make of the above observation regarding the path following by illuminants is to apply this additional constraint to colour constancy algorithms as extra information that can be brought to bear. We show that the specular-locus thus found does help in discovering the lighting in a scene. Moreover, since we know the path that illuminants would take depending on the colour temperature T , we can re-light a scene simply by changing T and thus moving along the locus. Using measured data for changing lights for static scenes we show below that this shift in lighting is indeed accurate.

The history of using specularities to discover the illuminant is lengthy, and here we simply highlight some key contributions used in this paper. Shafer [1] introduced the widely used and quite effective dichromatic model of reflectance for dielectric materials, wherein surface reflectance consists of (i) a diffuse ('body') component that depends on subsurface material properties of a reflecting surface and (ii) a specular ('surface') component

that depends on the air-surface interface layer and not the body-reflectance properties. The diffuse component is responsible for generating the colour and shading for an object and the specular component is responsible for highlights. For a dielectric (e.g., plastics) the neutral-interface model [2] states that the colour of the specular contribution is approximately the same as the colour of the illuminant itself. However, simply taking specular colour as identical with light colour is insufficient: typically, specular reflection looks white to the viewer (for dielectric materials), but in fact a careful inspection of specular pixels shows that the body colour is still present to some degree.

Klinker et al. [3] showed that when the diffuse colour is constant over a surface, the colour histogram of its image forms a T-shaped distribution, with the diffuse and specular pixels forming linear clusters. They used this information to estimate a single diffuse colour. Therefore in order to use this principle, their approach needed to segment an image into several regions of homogeneous diffuse colour. Moreover, Lee [4] proposed a method which uses specularities to compute illumination by using the fact that in the CIE chromaticity diagram [5] the coordinates of the colours from different points from the same surface will fall on a straight line connected to the specular point. This is the case when the light reflected from a uniform surface is an additive mixture of the specular component and the diffuse component. This seminal work initiated a substantial body of work on identifying specular pixels and using these to attempt to discover the illuminant [6, 7]. Another approach extending these algorithms is to define a constraint on the possible colours of illumination, making estimation more robust [8, 9].

Finlayson and Drew [10] used 4-dimensional images (more colours than R,G,B) formed by a special 4-sensor camera. They first formed colour ratios to reduce the dimensionality to 3 and to eliminate light intensity and shading; then projecting log values into the plane orthogonal to the direction in the 3-D space corresponding to a lighting change direction they arrived at generalized colour 2-vectors independent of lighting. They noted that in the 2-space, specularities are approximately linear streaks pointing to a single specular point. Therefore they could remove specularities by the simple expedient of replacing each 2-D colour by the maximum 2-vector position at its particular direction from the specular point. Note, however, that in [10] the authors were constrained to using a *four*-sensor camera. Here we relax that necessity by adding a more complete camera calibration phase.

In [11], Lu and Drew carried out an analysis again based on the formulation in [10], but in 3-D rather than 4-D and using an additional image generated by imaging a with-flash exposure in addition to an image with no flash. The addition of an extra image means that by subtracting the images an estimate of illuminant colour temperature can be established based on closeness to a predetermined set of clusters for different lights in a log-chromaticity space, using the mean over the image in that space compared to the clusters.

In this paper we present a new camera calibration method aimed at finding a specular-point locus in the log-chromaticity colour feature space, for daylight illuminants. We prove that, in a simplifying model for image formation under non-fluorescent illumination, any candidate illuminants for an image generated by a specific camera must lie on a line in log-log chromaticity space if we use a geometric mean to normalize colour. This has the consequence that ordinary r, g chromaticities formed by dividing by the sum $R + G + B$ must lie on a specific curve. To support these theoretical considerations, we demonstrate the applicability of the line in log chromaticity space for several different datasets and, as applications, we use the resulting curve for illumination recovery and re-lighting with a different illumination.

In essence, we are proposing a type of new colour constancy algorithm, one that uses a camera calibration. Many colour constancy algorithms have been proposed (see [12, 13] for an overview). The foundational colour constancy method, the so-called White-Patch or Max-RGB method, estimates the light source colour from the maximum response of the different colour channels [14]. Another well-known colour constancy method is based on the Grey-World hypothesis [15], which assumes that the average reflectance in the scene is achromatic. Grey-Edge is a recent version of the Grey-World hypothesis that says: the average of the reflectance differences in a scene is achromatic [16]. Finlayson and Trezzi [17] formalize grey-based methods by subsuming them into a single formula

using the Minkowski p-norm. The Gamut Mapping algorithm, a more complex and more accurate algorithm, was introduced by Forsyth [18]. It is based on the assumption that in real-world images, for a given illuminant one observes only a limited number of colours. Several extensions have been proposed [19–23].

The paper is organized as follows: To begin, in §2 we discuss the underlying assumptions that allow us to create a simplified model of colour image formation. Then in §3 we examine how the simplified model plus an offline calibration of the camera can be used to analyze the specular highlights. We propose a specular-point locus in chromaticity space in §4 based on the calibration for each camera. In §5 and §6 we use the proposed illuminant locus to demonstrate its applicability in two application areas: illuminant identification, and image re-lighting. In §7 we introduce a method to generate a matte image using our estimated illuminant, giving a specular-free image. Finally, we conclude the paper in §8.

2. Image Formation

To generate a simplified image formation model we apply the following set of simplifying assumptions (cf. [24]): (1) illumination is Planckian or is sufficiently near the Planckian locus that a blackbody radiator forms a reasonable approximation for this use [25]; (2) surfaces are dichromatic [1]; and (3) RGB camera sensors are narrowband or can be made sufficiently narrowband by a spectral-sharpening colour-space transform [26].

Thus we begin by considering a narrowband camera, with three sensors. Note again that in [10] the authors were constrained to using a *four*-sensor camera. Here we relax that necessity by adding a more complete camera calibration phase for a camera with only three sensors.

Real camera sensor curves are not in fact narrowband: Below, we investigate how the assumption of Planckian lighting impacts models of image formation by making use of a 3-sensor delta-function sensitivity camera. It is evident that real sensors are far from idealized delta functions: each is typically sensitive to a wavelength interval over 100nm in extent. Nevertheless, as we shall see, they behave sufficiently like narrowband sensors for our theory to work and moreover this behaviour could be promoted by carrying out calculations in an intermediate spectrally sharpened colour space [26].

Now let us briefly examine image formation in general for a dichromatic reflectance function comprising Lambertian and specular parts. For the Lambertian component, suppose there are $i = 1..L$ lights, each with the same SPD $E^i(\lambda)$ (e.g., an area source) given by Wien’s approximation of a Planckian source [5]:

$$E^i(\lambda) = I^i c_1 \lambda^{-5} e^{-c_2/(\lambda T_i)}, \quad c_1 = 3.74183 \times 10^{16}, \quad c_2 = 1.4388 \times 10^{-2} \quad (1)$$

with distant lighting from lights in normalized directions \mathbf{a}^i with intensities I^i (the constant c_1 determines the units). If the surface projecting to retinal point \mathbf{x} has spectral surface reflectance $S(\lambda)$ and normal \mathbf{n} then, for a delta-function narrowband sensor camera with spike sensor sensitivities $Q_k(\lambda) = q_k \delta(\lambda - \lambda_k)$, $k = 1..3$, the 3-vector RGB response R_k is

$$\begin{aligned} R_k &= \sum_{i=1}^L \mathbf{a}^i \cdot \mathbf{n} \int E^i(\lambda) S(\lambda) Q_k(\lambda) d\lambda \\ &= \sum_{i=1}^L c_1 \mathbf{a}^i \cdot \mathbf{n} S(\lambda_k) I^i (\lambda_k)^{-5} e^{-c_2/(\lambda_k T_i)} q_k \\ &= \left[\sum_{i=1}^L (c_1 I^i \mathbf{a}^i) \right] \cdot \mathbf{n} S(\lambda_k) (\lambda_k)^{-5} e^{-c_2/(\lambda_k T)} q_k \quad \text{if all } T_i = T \\ &\equiv \tilde{\mathbf{a}} \cdot \mathbf{n} S(\lambda_k) \lambda^{-5} e^{-c_2/(\lambda_k T)} q_k, \quad k = 1..3 \end{aligned} \quad (2)$$

The above is the matte model employed. For the specular part, let us assume a specular model dependent on the

half-way vector \mathbf{n}_S between the illuminant direction and the viewer:

$$\mathbf{R}^{\text{Specular}} = \sum_{i=1}^L \mathbf{b}_S^i \Phi(\mathbf{n}_S^i \cdot \mathbf{n}), \quad (3)$$

where \mathbf{b}_S^i is the colour of the specularity for the i^{th} light. E.g., in the Phong specular model [27],

$$\Phi(\mathbf{n}_S^i \cdot \mathbf{n}) = (\mathbf{n}_S^i \cdot \mathbf{n})^p, \quad (4)$$

where a high power p makes a more focussed highlight.

Now in a neutral interface model [4], the colour of the specular term is approximated as:

$$\mathbf{b}_S^i \equiv \text{colour of the light.} \quad (5)$$

Hence for Lambertian plus Specular reflectance, we arrive at a simple model:

$$R_k = \left[\tilde{\mathbf{a}} \cdot \mathbf{n} S(\lambda_k) + \sum_{i=1}^L c_1 I^i \Phi(\mathbf{n}_S^i \cdot \mathbf{n}) \right] \lambda_k^{-5} e^{-c_2/(\lambda_k T)} q_k. \quad (6)$$

For each pixel at a retinal position \mathbf{x} , the second term in the brackets is a constant, β say, that depends only on geometry and not on the light colour. Therefore we have

$$R_k = [\tilde{\mathbf{a}} \cdot \mathbf{n} S(\lambda_k) + \beta] \lambda_k^{-5} e^{-c_2/(\lambda_k T)} q_k \quad (7)$$

with possibly several specular highlights on any surface ($\beta = \beta(\mathbf{x})$).

If we define

$$\alpha = \beta/(\tilde{\mathbf{a}} \cdot \mathbf{n}), \quad (8)$$

then our expression simplifies to:

$$R_k = (\tilde{\mathbf{a}} \cdot \mathbf{n}) [S(\lambda_k) + \alpha] \lambda_k^{-5} e^{-c_2/(\lambda_k T)} q_k \quad (9)$$

3. Specular-Point Line in Log Chromaticity Space

We note that dividing by a colour channel (green, say) removes the initial factor in eq. (9). We can divide instead by the geometric mean (cf. [10]) so as not to be forced to choose a particular normalizing channel. Define the mean R_M by

$$R_M = \sqrt[3]{\prod_{k=1}^3 R_k}. \quad (10)$$

Then we can remove light intensity and shading by forming a chromaticity 3-vector \mathbf{r} via

$$r_k = R_k/R_M, \quad k = 1..3. \quad (11)$$

Thus from eq. (9) we have

$$\log r_k = \log \left(\frac{s_k + \alpha}{s_M + \alpha} \right) + w_k + (e_k - e_M) \frac{1}{T}, \quad k = 1..3, \quad (12)$$

where we simplify the expressions by defining some short-hand notations as follows:

$$\begin{aligned} s_k &= S(\lambda_k); v_k = \lambda_k^{-5} q_k; v_M = \left\{ \prod_{j=1}^3 \lambda_j^{-5} q_j \right\}^{1/3}, w_k = \log(v_k/v_M) \\ e_k &= -c_2/\lambda_k; e_M = (-c_2/3) \sum_{j=1}^3 (1/\lambda_j), \end{aligned} \quad (13)$$

and we define an effective geometric-mean-respecting value s_M by setting

$$(s_M + \alpha) \equiv \left\{ \prod_{j=1}^3 (s_j + \alpha) \right\}^{1/3}$$

In the case of broad-band sensors we replace some of the definitions in eq. (12) above by values that are equivalent for delta-function cameras but are appropriate for real sensors (extending definitions in [10]):

$$\begin{aligned} \sigma_k &= \int q_k(\lambda) d\lambda, \\ e_k &= (1/\sigma_k) \int -(c_2/\lambda) q_k(\lambda) d\lambda, \\ e_M &= (1/3) \sum_{j=1}^3 e_k, \\ s_k &= (1/\sigma_k) \int S(\lambda) q_k(\lambda) d\lambda, \\ v_k &= \int \lambda^{-5} q_k(\lambda) d\lambda \end{aligned} \tag{14}$$

The meaning of eq. (12) is that the log of the chromaticity is given by: (i) A term consisting of the matte-surface term s_k combined with a term α , a scalar at each pixel that is the specular contribution; (ii) a constant 3-vector offset term, w_k , which is a characteristic of the particular camera; and (iii) a term equal to the product of a ‘‘lighting-change’’ 3-vector ($e_k - e_M$), also characterizing the camera, times the inverse of the correlated colour temperature T encapsulating the colour of the light.

Thus as the light colour (i.e., T) changes, say into a shadow or because of inter-reflection, the log-chromaticity at a pixel \mathbf{x} simply follows a straight line in 3-space (as temperature T changes), along the light-change direction ($e_k - e_M$), even including the specular term α . For a fixed T , if α changes on a patch with reflectance vector s_k , then the plot of $\log \mathbf{r}$ will be a curved line.

In this paper, we mean to calibrate the camera so as to recover (a projection of) both this light-change vector as well as the constant additive term w_k . The difference from previous work [10] is as follows.

In the method [10], going over to a chromaticity space meant that 4 dimensions were reduced to 3. Then in that 3-space, light-change vector ($e_k - e_M$) was obtained as the first eigenvector of mean-subtracted colour-patch values. To then go over to a 2-space, log-chromaticity values were then projected onto the subspace orthogonal to 3-D light-change vector. This meant that all lighting colour and strength were projected away. In that plane, the illuminant, and consequently the specular point as well, were always located in precisely the same spot. It was argued that, at a highly specular point in an input image, the pixel values would essentially consist of the specular point and thus one could derive that point from training images. Then forming radii from that specular spot out to the least-specular pixel position effectively removed specularities.

Here, in contrast, we start with 3-D colour values, rather than 4-D ones, and so chromaticity vectors are effectively 2-D. Now calibration of the camera is used to provide both a value of the offset term w_k in eq. (12) as well as of the lighting-colour-change vector ($e_k - e_M$).

For specular pixels, there is no surface term s_k above in eq. (12), and $\log(\alpha/\alpha) = 0$, so the value of this log-geometric-mean chromaticity at a purely specular pixel becomes the simpler form

$$\log r_k = w_k + (e_k - e_M) \frac{1}{T}, \quad k = 1..3, \tag{15}$$

Thus as T changes we have a line, in a 2-D colour space, whereon any specular point must lie. To determine just where it does lie, we form an objective function measure, which is in fact minimized provided we choose the correct value of T : an example of such a measure is given below in §5.A. Hence we recover the temperature T and therefore the light colour. Moreover, since we have an illuminant locus we can go on to re-light images by moving the illuminant along the locus obtained during the camera calibration phase. Such re-lit images are shown below in §6 where images are shown as they would appear under a different colour temperature.

Note that although we work with 3-vectors, the step of division by the geometric mean creates $\log \mathbf{r}$ vectors that lie on a plane: they are all orthogonal to the vector $(1, 1, 1)^T$ — in fact, each of the three terms in eq. (12) lies in this plane. Thus the components are not independent.

4. Recovery of Specular-Point Locus

To find the vector $(e_k - e_M)$, $k = 1..3$ we image matte Lambertian colour patches. Here we use the 18 non-grey patches of the Macbeth ColourChecker [28]. We form $\log r_k$ values using temperatures T from 5500°K to 10500°K.

According to eq. (12) (with no specular contribution), for each surface we should see a set of points in 3-space that falls on a straight line along $(e_k - e_M)$. Thus for each surface, if we then subtract the mean, in each channel k of $\log r_k$, we see a set of nearly coincident lines through the origin.

Therefore, as pointed out in [25] (in a 2-D setting like eq.(12) but with $k = 1..2$), we can find vector $(e_k - e_M)$ by forming the covariance matrix of mean-subtracted $\log r_k$ values and calculating eigenvectors. The first eigenvector is the desired approximation of direction $(e_k - e_M)$.

To derive the offset term w_k , we utilize the recovered normalized version of vector $(e_k - e_M)$ and image two lights (below) to determine the scaling along the inverse-temperature line.

Since we know that our colour features lie on the plane perpendicular to the unit vector $\mathbf{u} = 1/\sqrt{3}(1, 1, 1)^T$, to simplify the geometry we first rotate all our log-chromaticity vector coordinates into that plane by forming the projector P_u onto the \mathbf{u} direction. 2-D coordinates χ are formed by multiplication of the rotation matrix U from the eigenvector decomposition of the projector $P_u^\perp = I - P_u$ onto the plane:

$$P_u^\perp = U^T \text{diag}(1, 1) U, \quad U \text{ is } 2 \times 3. \quad (16)$$

We denote 2-vectors in this 2-D space as χ . And, explicitly, we form 2-vectors in the plane by

$$\chi = U \log \mathbf{r} \quad (17)$$

Now suppose that in the 2-D coordinates χ , two lights E_1 and E_2 produce vectors χ^{E_1} and χ^{E_2} : for each light we form chromaticity (11), take logs, and then project via (17). Consider the recovered *normalized* light-change direction vector, projected into this plane: define the 3-vector \mathbf{e} as having components $(e_k - e_M)$, and denote its unit 2-vector projection as $\hat{\xi}$. Note that we recover only a *normalized* version of \mathbf{e} from our SVD analysis of imaged colour patches, with the norm unknown. That is, we work in the plane by rotating with U , and further normalize that projected 2-vector, giving a known, normalized, 2-vector $\hat{\xi}$ from our calibration.

Also, denote by $\boldsymbol{\eta}$ the projected vector w_k : this is what we aim to recover.

$$\begin{aligned} \hat{\xi} &= (U\mathbf{e})/\nu, \quad \text{where } \nu \equiv \|U\mathbf{e}\|, \\ \boldsymbol{\eta} &= U\mathbf{w}. \end{aligned}$$

Then the 2-vector coordinates for the two lights E_i , $i = 1..2$ are

$$\chi_\mu^{E_i} = \eta_\mu + \nu \hat{\xi}_\mu / T_i, \quad i = 1..2, \quad \mu = 1..2 \quad (18)$$

where ν is an unknown scale, and T_i are known colour-temperatures. Note that since we are imaging lights, not surfaces, the surface term s_k in eq. (12) is not present.

Forming the difference 2-vector $(\chi^{E_2} - \chi^{E_1})$, we obtain a result involving only the normalized direction $\hat{\xi}$. So we can determine the norm ν if we know T_1 and T_2 . For consider the difference 2-vector

$$\chi_\mu^{E_1} - \chi_\mu^{E_2} = \nu \hat{\xi}_\mu \left(\frac{1}{T_1} - \frac{1}{T_2} \right) \quad (19)$$

Even from these two data points we can easily determine the normalized vector $\hat{\xi}$ since it is simply given by the direction of the difference in χ . Since we know T_1, T_2 , the norm ν thus falls out of eq. (19).

Finally, subtracting the term $\nu\hat{\xi}_\mu/T_i$, $i = 1, 2$, from each of the two χ vectors and taking the mean, we recover the offset term η .

Let us denote by ξ the product $\nu\hat{\xi}$, so using this vector and the offset η we arrive at a line (for this particular camera calibrated as above) parametrized by temperature T that must necessarily be traversed by any candidate specular point:

$$\chi = \eta + (1/T)\xi \quad (20)$$

In summary, the calibration algorithm proposed is expressed in algorithm 1.

Algorithm 1 Proposed Camera Calibration

Colour target:

Record RGB responses R_k , $k = 1..3$ (reflected from colour target)

for several lights \rightarrow each pixel follows a parallel straight line;

calculate geometric mean at each pixel from eq. (10).

Derive geometric-mean-based chromaticity 3-vector \mathbf{r} from eq. (11), and take logarithms.

Find 3-vector $(e_k - e_M)$ as first eigenvector for $\log \mathbf{r}$ values, mean-subtracted

for each colour patch.

For illuminants $E(\lambda)$, characterized by their known temperatures T

(in a light-box, for example):

Derive $\log \mathbf{r}$ as above, for light reflected from a grey patch.

Project $\log \mathbf{r}$ onto plane orthogonal to $(1, 1, 1)$ via eq. (17), forming 2-D coordinates χ .

Subtracting pairs of χ values for known values T , find 2-D projected light-change vector ξ via eq. (19).

Using ξ , find mean value of camera offset vector η over χ vectors used, eq. (20).

As set out in algorithm 1, a more accurate way to recover the offset term η and the vector ξ is to utilize several different known illuminants and capture them using the camera to be calibrated: lights should approximately lie on a straight line in χ space. Then line parameters η and ξ , as well as outliers, can be recovered using a robust regression method such as the Least Median of Squares (LMS) [29].

We shall find in the following sections that the offset η and the vector ξ are all the calibration information that we need for different applications such as illuminant identification and re-lighting.

4.A. Real Images

The image formation theory used is based on three idealized assumptions: (1) Planckian illumination, (2) dichromatic surfaces; and (3) narrowband camera sensors. To determine if real images stand up under these constraints and generate the needed straight line in 2-D colour space, we make use of datasets of measured images [30, 31]. Fig. 1 displays measured illuminant points in χ space for 86 scenes captured by a high-quality Canon DSLR camera for 86 different lighting conditions [30]. Notwithstanding the fact that the camera sensors are not narrowband and illuminants are not perfectly Planckian, we can see that these illuminants do indeed approximately form a straight line, thus justifying the suitability of the theoretical formulation.

Since we assume that lights can be characterized as Planckian, we expect that severely non-Planckian lights will form outliers to the straight-line path determined. Figs. 2(a,b) demonstrate that this is indeed that case. Here we

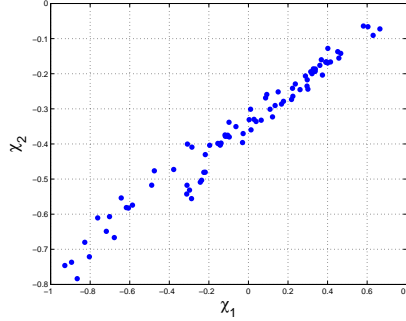


Fig. 1. 86 illuminants for Canon camera in χ space [30]. Note that these illuminants do approximately follow a straight line.

show illuminant points transformed to 2-D χ space for 98 images consisting of measured images of 9 objects that are specifically selected to include substantial specular content, under different illumination conditions [31]. In this dataset, illuminants for 26 of the images are fluorescent (Sylvania Warm White Fluorescent(WWF), Sylvania Cool White Fluorescent (CWF) and Philips Ultralume Fluorescent(PUF)). These show up in Fig. 2(a) as outlier points. Fig. 2(b) shows that the robust LMS method correctly identifies these points as outliers and thus does not include them in calculating line parameters.

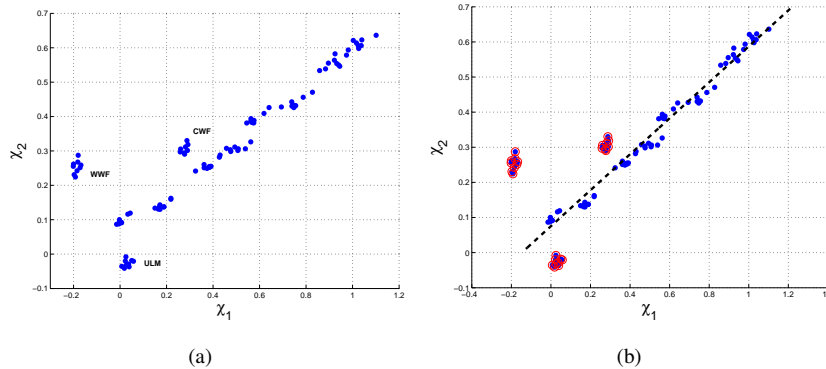


Fig. 2. (a): 98 illuminants for images containing significant specular content [31], plotted in 2-D χ colour space. Note clusters of points that arise from fluorescent illuminants (WWF, CWF, ULM). (b): Outliers automatically determined by LMS regression are shown using a red circle, and the regression line is shown as black dashed.

5. Illuminant Identification

Our camera calibration process has generated a locus in chromaticity space that candidate natural daylight illuminations will follow. In this section we show how for a new image we can identify a point on this locus as an estimate of the illuminant.

Recently, Drew et al. [32,33] presented an illuminant estimation method based on a planar constraint. This stated that for near-specular pixels, Log-Relative-Chromaticity (LRC) values are orthogonal to the light chromaticity: they showed that if one divides image chromaticity by illuminant chromaticity, then in a log space the resulting set of 3-vectors are approximately planar, for near-specular pixels, and orthogonal to the lighting — for the correct

choice of the illuminant only. Hence they propose an objective function based on this planar constraint which is minimized for the correct illuminant.

Here, we utilize this daylight illuminant planar constraint by further constraining the light to lie on the daylight locus we have derived above. The locus provides an additional constraint on the illuminant and hence improves the estimate.

To begin, we briefly recapitulate below the derivation of this planar constraint.

5.A. Plane Constraint

Suppose we rewrite eq. (9) for the 3-vector RGB response \mathbf{R} , here relinquishing the requirements that lighting be Planckian and sensors be narrowband, but instead applying the different simplifying assumption that matte pixel 3-vector RGB triples be a component-wise product of a light 3-vector ϵ_k , $k = 1..3$, and a surface triple ς_k [34]. Here, ς_k is the reflectance at a pixel under equi-energy white light.

Adding a Neutral Interface Model term [4] for specular content, as in eq. (7), we have approximately

$$R_k \simeq \frac{\kappa \varsigma_k \epsilon_k}{q_k} + \beta \epsilon_k \quad (21)$$

where κ is shading. E.g., for Lambertian matte shading κ equals lighting-direction dotted into surface normal. Here, q_k is again a triple giving the overall camera sensor strength [35]; β represents the amount of specular component at that pixel. The value of β for a pixel will depend upon the lighting direction, the surface normal, and the viewing geometry [1]. Let us lump values $\kappa \varsigma_k / q_k$ into a single quantity and for convenience call this simply ς_k . Now we have

$$R_k = \varsigma_k \epsilon_k + \beta \epsilon_k \quad (22)$$

Instead of the geometric-mean based chromaticity \mathbf{r} in eq. (11), let us make use of the standard L_1 -norm based chromaticity [5]

$$\boldsymbol{\rho} = \{R, G, B\} / (R + G + B) \quad (23)$$

Thus here we have

$$\rho_k = \frac{\varsigma_k \epsilon_k + \beta \epsilon_k}{\sum_{j=1}^3 (\varsigma_j \epsilon_j + \beta \epsilon_j)} \quad (24)$$

Let us define the Log-Relative-Chromaticity (LRC) as the above chromaticity divided by the chromaticity for the lighting itself, ρ_k^ϵ . The planar constraint [32] says that for near-specular pixels, LRC values are orthogonal to the light chromaticity, provided we have chosen the correct illuminant to divide by.

To see how this constraint arises, form the LRC, which we denote as ψ_k :

$$\psi_k = \log \left(\frac{\rho_k}{\rho_k^\epsilon} \right) = \log \left(\frac{\varsigma_k \epsilon_k + \beta \epsilon_k}{\sum_{j=1}^3 (\varsigma_j \epsilon_j) + \beta \sum_{j=1}^3 \epsilon_j} \cdot \frac{\sum_{j=1}^3 \epsilon_j}{\epsilon_k} \right) = \log \left(\frac{\varsigma_k + \beta}{\frac{(\sum_j \varsigma_j \epsilon_j)}{E} + \beta} \right) \quad (25)$$

For convenience, now define $E \equiv \sum_{j=1}^3 \epsilon_j = |\boldsymbol{\epsilon}|$ where $|\cdot|$ is the L_1 norm.

Near a specular point, we can take the limit as $(1/\beta) \rightarrow 0$. Let $\alpha = 1/\beta$. Then in the limit, ψ goes to

$$\psi_k = \lim_{\alpha \rightarrow 0} \log \left\{ (\alpha \varsigma_k + 1) / \left(\alpha \sum_j (\varsigma_j \epsilon_j) / E + 1 \right) \right\} \simeq \alpha \left(\varsigma_k - \frac{\sum_j \varsigma_j \epsilon_j}{E} \right) \quad (26)$$

The above is the Maclaurin series, accurate up to $O(\alpha^2)$. By inspection, we have that the LRC vector, ψ_k , is orthogonal to the illuminant vector: $\sum_{k=1}^3 \psi_k \epsilon_k = 0$, and hence also orthogonal to the illuminant chromaticity, $\sum_{k=1}^3 \psi_k \rho_k^\epsilon = 0$.

The planar constraint therefore suggests finding which illuminant amongst several candidates is the correct choice, for a particular image, by minimizing the dot-product over illuminants, for pixels that are likely near-specular [32]. Define ζ as the dot-product between ψ and the chromaticity for a candidate illuminant, with ζ formed by dividing by this same illuminant chromaticity:

$$\zeta = -\psi \cdot \rho^e = -\log(\rho / \rho^e) \cdot \rho^e \quad (27)$$

Then we seek to solve an optimization as express in algorithm 2

Algorithm 2 Illumination Estimation by Zeta using Optimization

$$\begin{aligned} \text{Minimize} \quad & \min_{\rho^e} \sum_{\psi \in \Psi_0} |\zeta| \\ \text{subject to} \quad & \sum_{k=1}^3 \rho_k^e = 1, 0 < \rho_k^e < 1, k = 1..3 \end{aligned} \quad (28)$$

where Ψ_0 is a set of pixel dot-product values with the candidate illuminant chromaticity ρ^e that are likely to be near specular, e.g. those in the lowest 10-percentile.

To include the Daylight Locus constraint, for a camera calibrated as above in algorithm 2, we consider only natural illuminants lying on the curve (20).

5.B. Experimental Results

We apply our proposed method to two different real-image datasets [31, 36] and compare our results to other colour constancy algorithms. The motivation here is to investigate whether the derived daylight locus correctly helps identify illuminants that are indeed daylights. We show that this is the case.

5.B.1. Laboratory Images

Our first experiment uses the Barnard dataset [31], denoted here as the SFU Laboratory dataset (introduced above in §4.A). This contains 321 measured images under 11 different measured illuminants. The scenes are divided into two sets as follows: minimal specularities (22 scenes, 223 images – i.e., 19 missing images); and non-negligible dielectric specularities (9 scenes, 98 images – 1 illuminant is missing for 1 scene). In this dataset the illuminant for 86 of the images are fluorescents. To compare to other colour constancy methods, we consider the following algorithms: White-Patch, Grey-World, and Grey-Edge implemented by [16]. For Grey-Edge we use optimal settings, which differ per dataset [37] ($p = 7$, $\sigma = 4$ for the SFU Laboratory dataset and $p = 1$, $\sigma = 1$ for the GreyBall dataset below). We also show the results provided by Gijsenij et al. [22] for pixel-based gamut mapping, using the best gamut mapping settings for each dataset.

How the daylight locus information is used is as an additional constraint to the optimization (28), whereby candidate illuminants are restricted to the daylight locus determined by our calibration, for the camera used in taking images.

Table 1 lists the accuracy of the proposed method for the SFU Laboratory dataset [31], in terms of the mean and median of angular errors, compared to other colour constancy algorithms applied to this dataset. Since the daylight locus is designed for natural lights (Planckian illuminants) and not fluorescents, we expect performance to be better for non-fluorescents, and this is indeed the case for the 86 scenes imaged under fluorescent lighting. As well, we break out results for all methods for non-fluorescent illuminants (235 images). The results show that in fact using the daylight locus outperforms all other methods in terms of median error, notwithstanding the fact that it is a much less complex method than the gamut-mapping algorithms and does not require any tuning parameters.

The main conclusion to be drawn from this experiment is that the daylight locus does aid a planar-constraint driven illuminant identifier when illuminants are indeed natural lights. This justifies the suitability of our daylight-locus formulation as a useful physics-based constraint of natural lighting.

Table 1. Angular errors for several colour constancy algorithms, for SFU Laboratory dataset [31].

Method	all		non-fluorescent	
	Median Er	Mean Er	Median Er	Mean Er
White-Patch	6.5°	9.1°	6.9°	9.9°
Grey-World	7.0°	9.8°	6.4°	9.4°
Grey-Edge ($p = 1, \sigma = 6$)	3.2°	5.6°	2.9°	5.3°
Gamut Mapping pixel ($\sigma = 4$)	2.3°	3.7°	1.8°	3.5°
Planar Constraint Search	1.9°	4.3°	1.9°	4.6°
Daylight Locus using Planar Constraint	2.4°	5.1°	1.6°	4.4°

5.B.2. Real-World Images

For a more real-world (out of the laboratory) image experiment we used GreyBall dataset provided by Ciurea and Funt [36]: this dataset contains 11346 images extracted from video recorded under a wide variety of imaging conditions. The images are divided into 15 different clips taken at different locations. The ground truth was acquired by attaching a grey sphere to the camera, displayed in the bottom-right corner of the image. This grey sphere must be masked during experiments.

Fig. 3(a) shows the illuminants for this image set, mapped into 2-D χ colour space eq. (17). We see that these illuminants do approximately follow a straight-line path in 2-space; the LMS-based robust regression method finds a straight-line regression line shown red-dashed. Transformed back into standard L_1 -norm based chromaticity space (23) the path is curved, as in Fig. 3(b).

Table 2 shows results for this dataset. We find that the Daylight Locus using the Planar Constraint does better than all the other methods save one: it is only bested by the far more complex Natural Image Statistics method [38]. This is a machine learning technique to select and combine a set of colour constancy methods based on natural image statistics and scene semantics. Again, we find that adding the Daylight Locus information improves the Planar Constraint approach since here lights used are natural daylights.

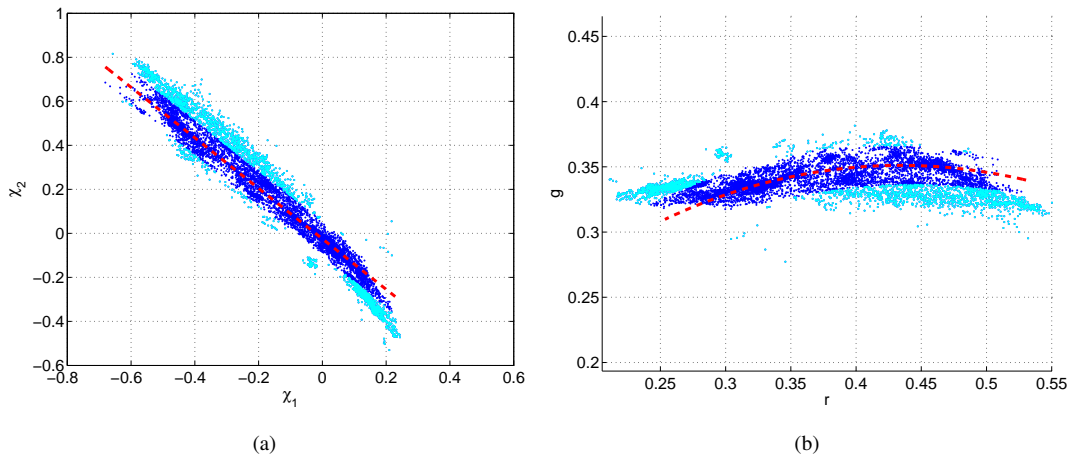


Fig. 3. (a): 11346 illuminants of GreyBall data set [36] in χ 2-space: they approximately follow a straight line locus. (b): The illuminants transformed back into a curve in L_1 -norm based chromaticity space.

Table 2. Angular errors for several colour constancy algorithms for GreyBall dataset [36].

Method	Median Er	Mean Er
White-Patch	5.3°	6.8°
Grey-World	7.0°	7.9°
Grey-Edge ($p = 1, \sigma = 1$)	4.7°	5.9°
Gamut Mapping pixel ($\sigma = 4$)	5.8°	7.1°
Natural Image Statistics [38]	3.9°	5.2°
Planar Constraint Search	4.6°	5.9°
Daylight Locus using Planar Constraint	4.1°	5.6°

6. Re-Lighting Images

We have shown that by means of calibrating the camera we can recover the specular point for a new image not in the calibration set. That is, the method recovers an estimate of the temperature T for the actual natural illuminant in a test image. Moreover, we have a curve that illuminants must traverse as the lighting colour changes. Consequently it should be possible to re-light an image by changing the position of the specular point along the curve, thus generating new images with a different illuminant.

If we again adopt the assumption that camera sensors are narrow-band, we can use a diagonal colour space transform [39] to move the image into new light conditions, via the following equation:

$$M = \text{diag}(\boldsymbol{\rho}^{e'}) \text{diag}(\boldsymbol{\rho}^e)^{-1} \tag{29}$$

$$\mathbf{R}' = \mathbf{R} M$$

where $\text{diag}(\boldsymbol{\rho}^e)$ is a 3×3 diagonal matrix with values from vector $\boldsymbol{\rho}^e$, and with $\boldsymbol{\rho}^e$ the current specular point and $\boldsymbol{\rho}^{e'}$ the new specular point; \mathbf{R} and \mathbf{R}' are the original and transformed RGB vectors for each image pixel.

Fig. 4 shows the same image for different Planckian illuminants from 1500°K to 10000°K, using the proposed re-lighting method. The method arguably produces reasonable output images corresponding to the colour of the lights involved.

In another experiment, we compare the error of using daylight locus for re-lighting, via eq. (29) compared to using the actual value of illuminants. Fig. 5 shows the same image transferred to other measured images, using their estimated illuminants on the daylight locus. In all, we generated re-lit images for a fixed object under 8 different illuminants (56 re-lightings). In terms of PNSR error for generated images compared to measured ones, we found a median PSNR value of 33.8dB, with minimum and maximum values of 28.2 and 43.5dB. These values demonstrate acceptable faithfulness of rendition for images under new lighting. QAs another comparison, instead of using illuminants on the locus we instead used actual measured illuminants in transforming the image via eq. (29). Now the min/median/max PSNR values are 28.2, 34.0 and 43.2, almost identical with those found using the illuminant approximation derived from the locus. This demonstrates that using the locus is nearly as good as using the actual illuminant, for this re-lighting task, with negligible difference in results.

7. Matte Image from Angle Image

We would like to generate a matte output image, which will then act as an invariant image free of shading and specularities (which could then be used as input to a segmentation scheme, for example). However, our specular-

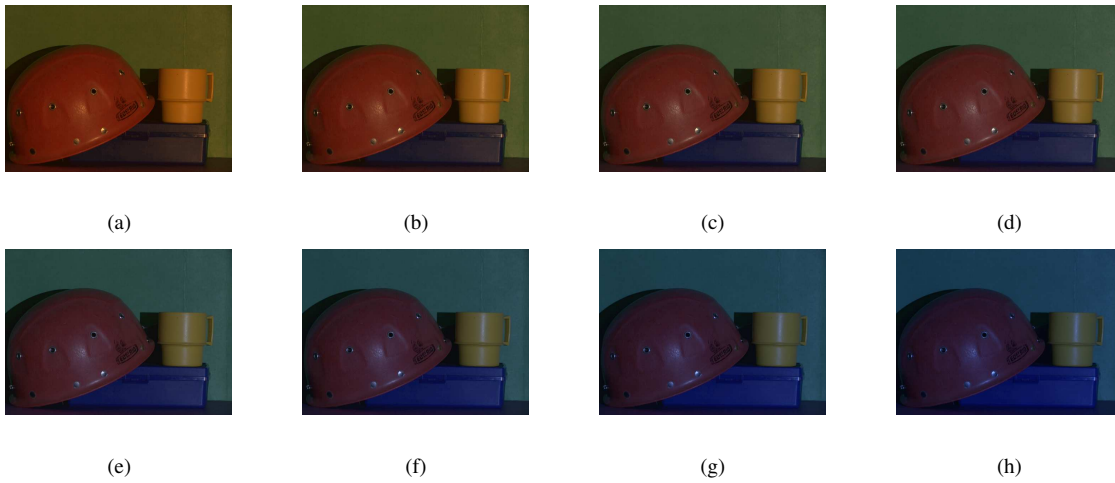


Fig. 4. (a-h): Images generated by re-lighting with Planckians of differing temperatures $T=1600^{\circ}\text{K}$, 1900°K , 2400°K , 2750°K , 3900°K , 4950°K , 6750°K , 10600°K .

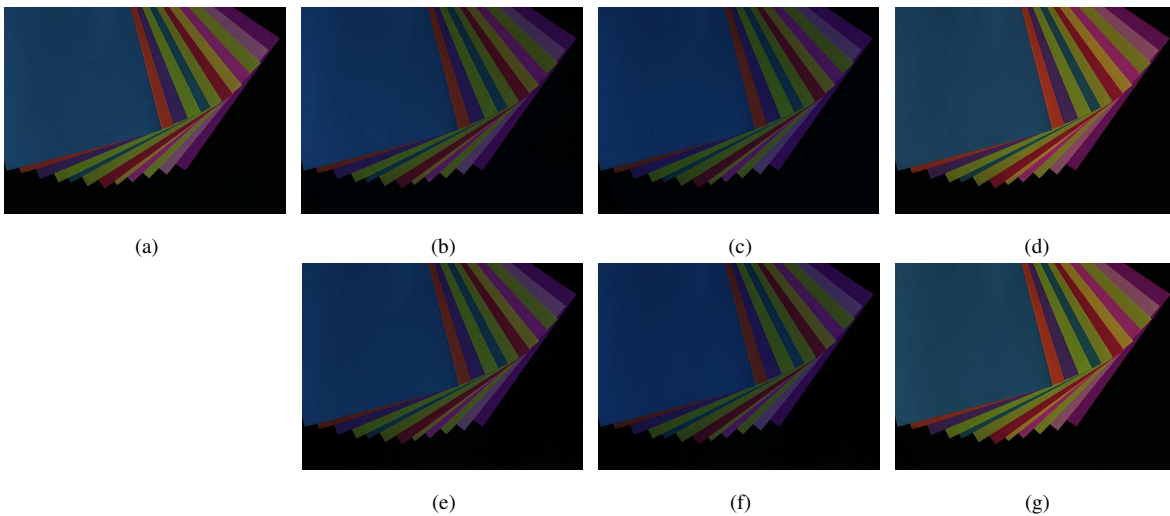


Fig. 5. (a-d): Input image; (e-g): Images generated by re-lighting of images (a) using (b-d) estimated illuminants on daylight locus. The PSNR for (e-g) are respectively: 42.3, 37.1 and 33.9.

invariant quantity is the angle from the recovered specular point, to each image pixel in feature space. However, this angle encapsulates hue information. The main point is that the angle from the specular point to the feature point of a pixel is approximately independent of the presence or absence of specular content at that pixel. Hence, if there is any structure in the image feature space χ from specular content, then by going over to this 2-D chromaticity space radii from the specular point will be in the same direction for pixels of the same body colour with or without specular content.

Based on the chromaticity-space model [4], a pixel value is a linear combination of the light colour and the matte colour, as measured by the camera, resulting in a line in chromaticity space starting from the matte point for any particular colour and leading towards the illuminant colour. Since we already know the light, assumed to be the colour of the specular point, we have this line direction for each pixel, leading from from specular point to that pixel. Moreover, these lines correspond to the angular values that we already assigned to each pixel. We can therefore consider the pixels with the same angular value as belonging to the same matte object — although in real images it is possible that two matte values fall on the same line toward the specular point. Here we initially simply take any such cases as belonging to the same matte value; however, below, considering spatial information we can in fact separate these two matte values from each other.

To make the calculation simpler we transform the chromaticity of the specular point to the origin and use polar coordinate (r, θ) . We discretize angle values by using $\lfloor \theta \rfloor$ to have 360 bins. Therefore for each chromaticity point v , we consider $(r_v, \theta_v) = \text{polar}(v - S)$, where S is the specular point.

The final step to generate a specularity-free colour image is to find a matte value for each pixel. We take the farthest-most pixel from the specular point (i.e., maximum radius r) for each θ as the matte colour (after removing outliers). So the matte colour for each pixel at that angle is identified with the farthest pixel. We call this process “angular projection to matte colour”. In other words we are projecting chromaticity points to the border of chromaticity values for each angle, considering the specular point as the center of projection:

$$\text{matte}(v) = \max_{\theta_u = \theta_v} \text{Index}(r_u) \quad (30)$$

Fig. 6 illustrates the projection for chromaticity points for a real image by angular projection to matte colour.

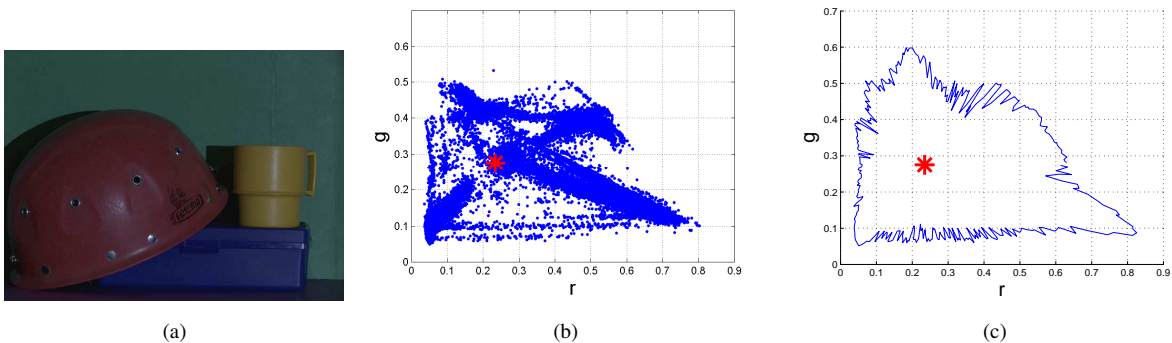


Fig. 6. (a): A real image. (b): Chromaticity points for (a); the red star is the correct specular point. (d): Angular projection to matte colour for image points.

The angular projection is more sensitive to noise the closer are image feature points to the specular point. Generally, because of noise angular projection to matte colour may completely fail for highlights. Hence we deal with the 10% of pixels that are close to each candidate specular point differently — we iteratively inpaint these pixels using matte colour data from neighbouring pixels that correspond to the same angular value (1-D inpainting). That is, we use voting based on the matte colour of the pixel’s neighbours: the new matte colour for that pixel will be the majority of its neighbours’ matte colour if it garners at least half of the votes.

A complete synthetic example consists of accurately modeled matte plus specular components. Here, let us consider a test image consisting of three shaded spheres (as in [10]), with surface colours equal to patches 1, 4, and 9 of the Macbeth ColourChecker [28] (dark skin, moderate olive green, moderate red), and under standard illuminant D65 (standard daylight with correlated colour temperature 6500K [5]) using the sensor curves for a Kodak DCS420 digital colour camera. If we adopt a Lambertian model then the matte image is as in Fig. 7(a). We now add a specular reflectance lobe for each surface reflectance function. We use the Phong illumination model [27], together with underlying matte Lambertian shading. Here, we use a Phong factor of 1 for the magnitude relative to matte. For the Phong power, we use a power of 20, where the inverse is basically roughness, 0.05. The matte image goes over to one with highlights as in Fig. 7(b). For our synthetic example, the resulting chromaticity image ρ is shown in Fig. 7(d). Comparing to the *input* chromaticity image in Fig. 7(c), we see that the algorithm performs very well for generating the underlying matte image — specularities in the center of each sphere are essentially gone. In comparison, Fig. 7(a) shows the theoretical, correct, matte image, which is indeed very close to the algorithm output in Fig. 7(a).

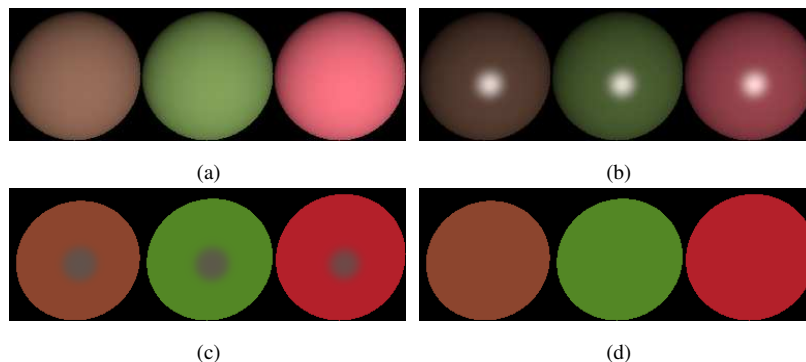


Fig. 7. (a): Ground-truth synthetic image of Lambertian surfaces under standard illuminant D65. (b): Image with specular reflection added. (c): The *input*(b) chromaticity image. (d): The chromaticity image resulting from angular projection to matte colour.

Fig. 8 shows results, including finding the specular point and generating a matte colour image, for 4 of input images: whereas the original images’ chromaticity clearly shows highlight effects and some shading, output for the proposed method effectively eliminates these effects.

8. Conclusion

In this paper we present a new camera calibration method aimed at recovering parameters for the locus followed by illuminants in a special 2-D chromaticity space. The objective is to discover the colour-temperature of the illuminant in the scene, for a new image not in the training set but captured using the calibrated camera.

As a testing method to verify the validity of the proposed locus idea, we compare illuminant recovery making use of the suggested locus as opposed to not using it. We determined that adding the locus constraint does indeed help identify the scene illuminant. While the effect is not large, nonetheless the experiments do provide a justification of the locus approach — a new insight in physics-based vision.

As an additional capability, we can subsequently generate a new version of the input image, shown as it would appear re-lit under new lighting conditions by considering different illuminant values as the illuminant moves along the specular-point locus.

In future work we will investigate how to make the method more robust to illuminants that differ more substantially from Planckians.

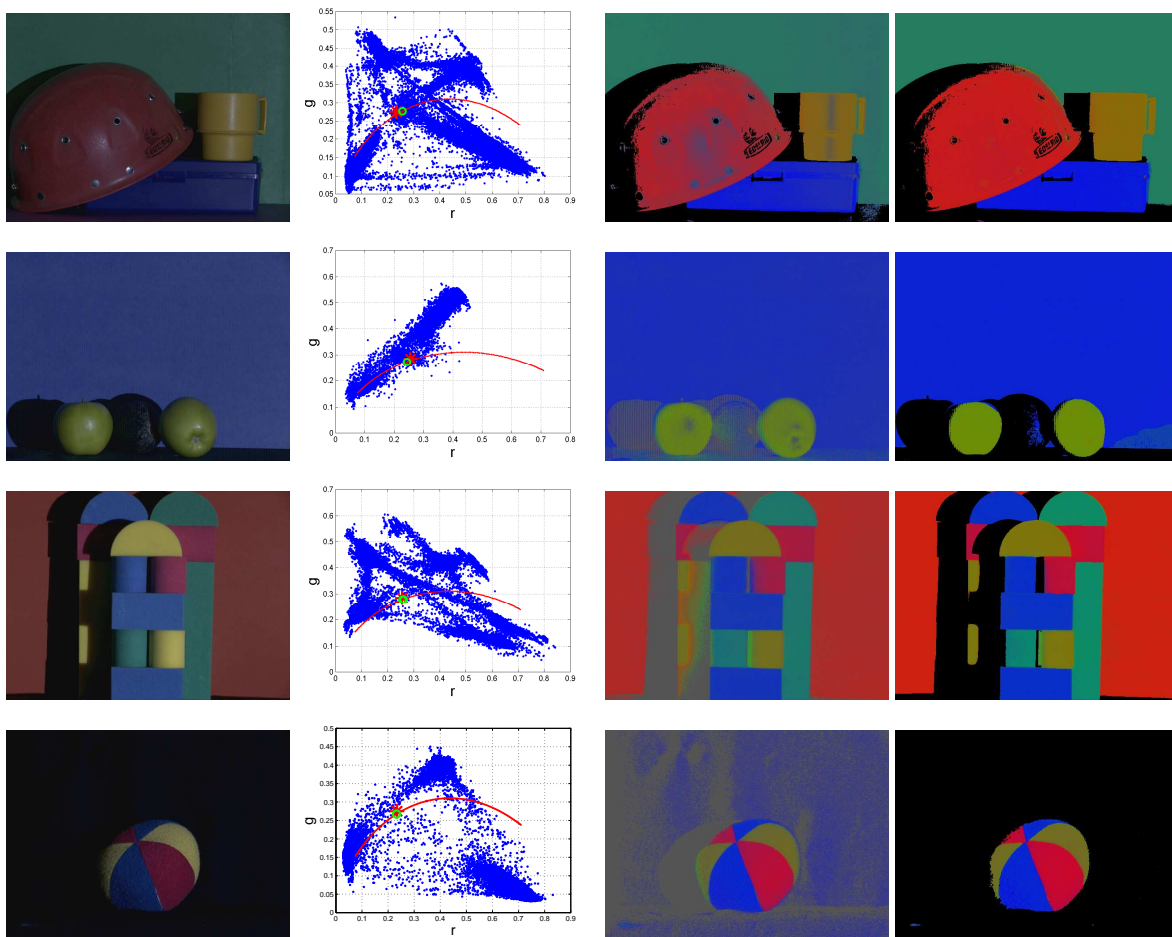


Fig. 8. Left column: Input image; Second column: chromaticity and illuminant estimate; Third column: input image chromaticity shows highlights; Fourth column: proposed method removes shading and highlights.

References

1. S. Shafer, "Using color to separate reflection components," *Color Research and Applications* **10**, 210–218 (1985).
2. H.-C. Lee, E. Breneman, and C. Schulte, "Modeling light reflection for computer color vision," *IEEE Trans. Pattern Analysis and Machine Intelligence* **12**, 402–409 (1990).
3. G. Klinker, S. Shafer, and T. Kanade, "The measurement of highlights in color images," *International Journal of Computer Vision* **2**, 7–32 (1988).
4. H.-C. Lee, "Method for computing the scene-illuminant chromaticity from specular highlights," *The Journal of the Optical Society of America A* **3**, 1694–1699 (1986).
5. W. Wyszecki and W. Stiles, *Color Science: Concepts and Methods, Quantitative Data and Formulas* (Wiley, New York, 1982), 2nd ed.
6. T. Lehmann and C. Palm, "Color line search for illuminant estimation in real-world scenes," *The Journal of the Optical Society of America A* **18**, 2679–2691 (2001).
7. R. Tan and K. Ikeuchi, "Separating reflection components of textured surfaces using a single image," *IEEE Transactions on Pattern Analysis and Machine Intelligence* pp. 178–193 (2005).
8. G. Finlayson and G. Schaefer, "Convex and non-convex illumination constraints for dichromatic color constancy," in "Proceedings of the IEEE Conference on Computer Vision and Pattern Recognition," (2001), pp. 598–605.
9. G. Finlayson and G. Schaefer, "Solving for colour constancy using a constrained dichromatic reflection model," *Int. J. Comput. Vision* **42**, 127–144 (2001).
10. G. Finlayson and M. Drew, "4-sensor camera calibration for image representation invariant to shading, shadows, lighting, and specularities," in "ICCV'01: International Conference on Computer Vision," (IEEE, 2001), pp. II: 473–480.
11. C. Lu and M. Drew, "Practical scene illuminant estimation via flash/No-flash pairs," in "Color Imaging Conference," (2006).
12. S. Hordley, "Scene illuminant estimation: past, present, and future," *Color Research and Application* **31**, 303–314 (2006).
13. A. Gijsenij, T. Gevers, and J. van de Weijer, "Computational color constancy: Survey and experiments," *IEEE Transactions on Image Processing* **20**, 2475–2489 (2011).
14. E. Land, "The retinex theory of color vision," *Scientific American* **237**, 108–128 (1977).
15. G. Buchsbaum, "A spatial processor model for object colour perception," *J. Franklin Inst.* **310**, 1–26 (1980).
16. J. van de Weijer and T. Gevers, "Color constancy based on the grey-edge hypothesis," in "Int. Conf. on Image Proc.," (2005), pp. II:722–725.
17. G. Finlayson and E. Trezzi, "Shades of gray and colour constancy," in "Twelfth Color Imageing Conference: Color, Science, Systems and Applications.," (2004), pp. 37–41.
18. D. Forsyth, "A novel approach to color constancy," in "Proceedings of the Int. Conf. on Computer Vision," (1988), pp. 9–18.
19. K. Barnard, "Improvements to gamut mapping colour constancy algorithms," in "European conference on computer vision," (2000), pp. 390–403.
20. G. Finlayson and S. Hordley, "Improving gamut mapping color constancy," *IEEE Transactions on Image Processing* **9**, 1774–1783 (2000).
21. G. Finlayson, "Color in perspective," *IEEE Transactions on Pattern Analysis and Machine Intelligence* **18**, 1034–1038 (1996).
22. A. Gijsenij, T. Gevers, and J. van de Weijer, "Generalized gamut mapping using image derivative structures

- for color constancy,” *International Journal of Computer Vision* **86**, 127–139 (2008).
23. H. Vaezi Joze and M. Drew, “White patch gamut mapping colour constancy,” in “Proceedings of IEEE Int. Conf. on Image Proc.”, (IEEE, 2012).
 24. G. Finlayson, S. Hordley, C. Lu, and M. Drew, “On the removal of shadows from images,” *IEEE Trans. Patt. Anal. Mach. Intell.* **28**, 59–68 (2006).
 25. G. Finlayson and S. Hordley, “Colour constancy at a pixel,” *The Journal of the Optical Society of America A* **18**, 253–264 (2001).
 26. G. Finlayson, M. Drew, and B. Funt, “Spectral sharpening: sensor transformations for improved color constancy,” *The Journal of the Optical Society of America A* **11**, 1553–1563 (1994).
 27. J. Foley, A. van Dam, S. Feiner, and J. Hughes, *Computer Graphics: Principles and Practice* (Addison-Wesley, 1990), 2nd ed.
 28. C. McCamy, H. Marcus, and J. Davidson, “A color-rendition chart,” *J. App. Photog. Eng.* **2**, 95–99 (1976).
 29. P. Rousseeuw and A. Leroy, *Robust Regression and Outlier Detection* (Wiley, 1987).
 30. P. Gehler, C. Rother, A. Blake, T. Minka, and T. Sharp, “Bayesian color constancy revisited,” in “CVPR’08: Computer Vision and Pattern Recognition,” (2008).
 31. K. Barnard, L. Martin, B. Funt, and A. Coath, “A data set for colour research,” *Color Research and Applications* **27**, 147–151 (2002).
 32. M. Drew, H. V. Joze, and G. Finlayson, “Specularity, the zeta-image, and information-theoretic illuminant estimation,” in “CPCV2012: European Conference on Computer Vision Workshop on Color and Photometry in Computer Vision,” (2012).
 33. M. S. Drew, H. R. V. Joze, and G. D. Finlayson, “The zeta-image, illuminant estimation, and specularity manipulation,” *Computer Vision and Image Understanding* **127**, 1–13 (2014).
 34. C. Borges, “Trichromatic approximation method for surface illumination,” *The Journal of the Optical Society of America A* **8**, 1319–1323 (1991).
 35. M. Drew and G. Finlayson, “Multispectral processing without spectra,” *The Journal of the Optical Society of America A* **20**, 1181–1193 (2003).
 36. F. Ciurea and B. Funt, “A large image database for color constancy research,” in “IS&T/SID Color Imaging Conference,” (2003), pp. 160–164.
 37. A. Gijsenij, “Color constancy : Research website on illuminant estimation,” <http://staff.science.uva.nl/~gijsenij/colorconstancy/index.html>.
 38. A. Gijsenij and T. Gevers, “Color constancy using natural image statistics and scene semantics,” *IEEE Transactions on Pattern Analysis and Machine Intelligence* **33**, 687–698 (2011).
 39. H. Chong, S. Gortler, and T. Zickler, “The von kries hypothesis and a basis for color constancy,” in “IEEE International Conference on Computer Vision,” (2007), pp. 1–8.